

Ultrafast Photo-induced Phase Transition in 2D MoTe₂

Bo Peng,^{1,2,3} Hao Zhang,^{1,*} Weiwen Chen,¹ Zhi-Jun Qiu,⁴ Hezhu Shao,⁵
Heyuan Zhu,¹ Bartomeu Monserrat,³ Desheng Fu,^{6,†} and Hongming Weng^{2,‡}

¹Key Laboratory of Micro and Nano Photonic Structures (MOE),
Department of Optical Science and Engineering, Fudan University, Shanghai 200433, China

²Beijing National Laboratory for Condensed Matter Physics,
and Institute of Physics, Chinese Academy of Sciences, Beijing 100190, China

³TCM Group, Cavendish Laboratory, University of Cambridge,
J. J. Thomson Avenue, Cambridge CB3 0HE, United Kingdom

⁴State Key Laboratory of ASIC & System, School of Information Science and Technology, Fudan University, Shanghai 200433, China

⁵Ningbo Institute of Materials Technology and Engineering, Chinese Academy of Sciences, Ningbo 315201, China

⁶Department of Electronics & Materials Sciences, Faculty of Engineering,
& Department of Optoelectronics and Nanostructure Science,

Graduate School of Science and Technology, Shizuoka University, Hamamatsu, 432-8561, Japan

Photo-induced phase transitions (PIPTs) provide an ultrafast, energy-efficient way for precisely manipulating the topological properties of transition-metal ditellurides, and can be used to stabilize a topological phase in an otherwise semiconducting material. By first-principles calculations, we demonstrate that the PIPT in monolayer MoTe₂ from the semiconducting 2H to the topological 1T' phase is driven purely by electronic excitations. The photo-induced electronic excitation changes the electron density, and softens the lattice vibrational modes. These pronounced softenings lead to structural symmetry breaking within sub-picosecond timescales, which is far shorter than the timescale of a thermally driven phase transition. The transition is predicted to be triggered by photons with energies over 1.96 eV, corresponding to an excited carrier density of $3.4 \times 10^{14} \text{ cm}^{-2}$, which enables a controllable phase transformation by varying the laser wavelength. Our results provide insight into the underlying physics of the phase transition in 2D transition-metal ditellurides, and show an ultrafast phase transition mechanism for manipulation of the topological properties of 2D systems.

The *photo-induced phase transition* (PIPT), which results from cooperative electron-lattice interactions through changing the electronic states of the solid transiently by photoexcitations¹, is completely different from thermally or pressure-induced phase transitions caused by spontaneous symmetry breaking. A PIPT not only allows us to access different hidden phases in the solid to explore anomalous properties absent in the ground state phase², but also enables precisely controllable phase transitions towards target structures with desired physical properties at high speeds³. Thus, the initial discovery of PIPT in organic charge transfer crystals has triggered great interest in a variety of fields⁴. Compared with the vast number of materials exhibiting thermodynamic phase transitions, there are still very few solids undergoing PIPT, and many investigations currently focus on bulk crystals possessing one-dimensional (1D) correlated electron chains in which PIPT may be easily triggered due to the inherent instabilities caused by electron-electron and electron-lattice interactions in these quasi-1D systems^{1,5}.

As an emerging platform for PIPT, two-dimensional (2D) layered transition-metal ditellurides exhibit polymorphisms with distinct physical properties⁶⁻⁸. Recent experimental evidence for a PIPT in MoTe₂ and WTe₂ shows that structural phase transitions often involve abrupt changes in the electronic structure accompanied by the emergence of novel topological states⁹⁻¹¹. For instance, in few-layer MoTe₂, an irreversible transition from a semiconducting hexagonal 2H phase to a topological distorted octahedral 1T' phase occurs under laser irradiation, which can be used to fabricate an ohmic heterophase homojunction with accurate control of micron-patterning in a desired area⁹. Such structural distortion re-

sults in an intrinsic band inversion between Te *p* and Mo *d* bands^{12,13}, enabling ultrafast manipulation of the topological properties. The topological phases also display gate-tunable superconductivity, providing a new platform to realize Majorana bound modes^{14,15}.

However, the microscopic nature of the phase transition remains unclear. Triggered by external stimulation by light, the system undergoes changes in temperature, strain, electronic excitation, chemical state and lattice vibrational modes. The transition may depend on one of these factors or on a combination of them^{9,16}. One proposal is that Te vacancies created by irradiation trigger the local phase transition^{9,17,18}. Other theoretical and experimental studies have argued that accumulated heat is a main driving force for the phase transition^{17,19}. Moreover, a strain-induced phase transition has been observed in monolayer MoTe₂^{20,21}, thus laser-induced thermal strain may also contribute to the observed phase transition. Yet another explanation is that it is the electronic excitation that plays a critical role in the phase transition^{22,23}. Overall, the transition mechanism is still debated.

Here, we demonstrate that the phase transition of monolayer MoTe₂ can be triggered by photoexcitation alone. Photoexcitation modifies the chemical bonds, resulting in a complete softening of the lattice vibrations that leads to spontaneous structural distortions with new equilibrium positions for the atoms. This structural transition takes place within one picosecond, far shorter than the timescale for the photoexcited electrons to transfer their energy to the lattice (about hundreds of ps²⁴). We also rule out a thermally-driven or a strain-induced phase transition under laser irradiation by studying the thermodynamic stability of 2H and 1T' MoTe₂ monolay-

ers. Our findings not only reveal the origin of the PIPT in 2D transition-metal ditellurides, but also provide new insight into the observed dynamic transitions in their 3D counterparts, another question that remains unclear^{10,25,26}.

All calculations are performed based on density functional theory (DFT) using the Vienna *ab-initio* simulation package (VASP)²⁷. In the excited state simulations, we mimick optical excitation by promoting valence electrons from high-lying valence band states to low-lying conduction band states^{28,29}, and the occupied conduction band is determined by energy conservation at photoexcitation energies E of 1.58 eV (785 nm), 1.96 eV (633 nm), 2.34 eV (532 nm), 2.42 eV (514 nm), and 2.63 eV (473 nm) (see ‘‘Computational Details’’ in SUPPLEMENTARY INFORMATION). We keep these occupancies fixed in the following calculations. This corresponds to the time domain of interest, namely, after the laser excited carriers populate the band edge states but before these carriers recombine or interact with various phonons. The excited electrons thermalize themselves within 20 fs, and the electron-hole recombination happens on the order of picoseconds, which is much larger than the phonon periods (discussed later in *Timescale of the phase transition*). Thus the number of excited electrons can be reasonably assumed to remain constant in the calculation. Indeed, such approach has been used to study the excited state of monolayer MoTe₂²².

The semiconducting 2H phase is characterized by a hexagonal $P\bar{6}m2$ unit cell with a trigonal prismatic arrangement of Te ligands around a central Mo atom. The 1T' phase possesses an orthorhombic $P2_1/m$ structure with a distorted octahedral coordination of the Mo atoms, in which the Te atoms in the two opposite planes stagger, resulting in a semi-metallic electronic structure with complex topological states³⁰. The crystal structures of 2H and 1T' MoTe₂ monolayers are shown in SUPPLEMENTARY INFORMATION.

Photo-induced change in the electronic state. Upon optical irradiation, electrons are excited in the 2H lattice, which may induce ultra-rapid bond dissociation²⁹. We firstly examine how the photoexcitation changes the electronic state in the system. Fig. 1 shows the electron localization function of 2H MoTe₂ at different photoexcitation energies. With increasing excitation energy, the red contours of the highly localized electrons around the Te atoms are shrunk [Fig. 1(b)], and the electrons in the Te layer become more localized. The change of electron distribution in the Mo layer is more distinct. As shown in Fig. 1(c), under an optical excitation of 1.58 eV, the electron distribution around Mo atoms changes from isolated triangles to connected hexagons. As the excitation energy increases to 1.96 eV, the electrons in the Mo layer are gathered between top and bottom Te atoms, and the in-plane triangles around Mo atoms appear once again, but with a reversed orientation, increasing the degeneracy of electronic states. As the excitation energy increases to 2.34 eV, the inverted-triangle region of the electron density is further shrunk. Thus the the degeneracy of electronic states is further increased. According to the Jahn-Teller theorem, degenerate electronic states are unstable³¹, and such degeneracies can be removed by structural distortions. As a result, irreversible displacements may be generated to induce phase transition.

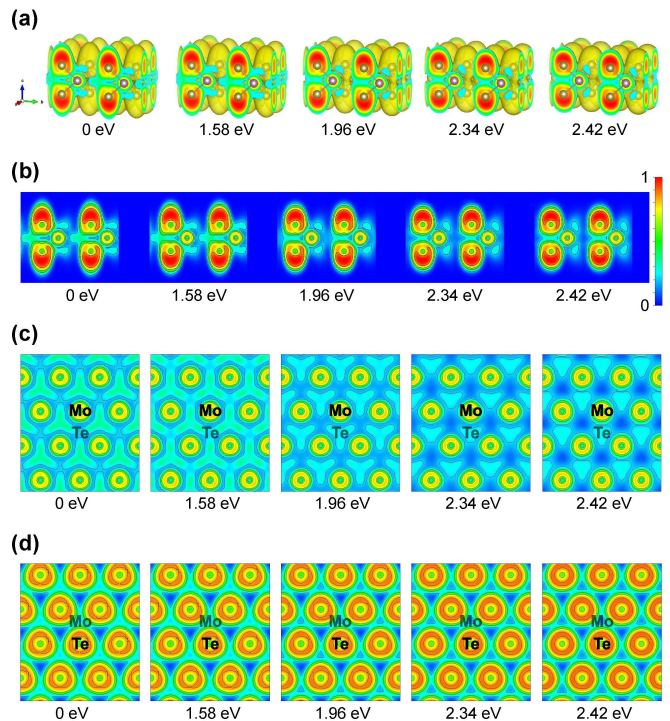


FIG. 1. (a) 3D, (b) side view, top view of (c) Mo layer and (d) Te layer of electron localization function of 2H MoTe₂ at different excitation energies. Electron localization function from 0 to 1 is shown by colours from navy to red. The isosurface for electron localization function in (a) is 0.2.

Photo-induced lattice mode softening. As discussed above, structural distortions may arise as a result of complete change of the electron density. We then examine the atomic displacements in the excited state to see whether (and how) a phase transition occurs. With D_{3h} point group, the irreducible representations of the vibrational modes in the 2H phase at the Γ point is expressed as³²

$$\Gamma_{2H} = E'' + A_1' + E' + A_2'' \quad (1)$$

The calculated phonon dispersion is shown in Fig. 2(a), and the calculated lattice mode frequencies are consistent with previous reports^{33,34}.

We then focus on three modes (E'' , E' and A_2'') corresponding to the three primary lattice distortions along the pathway from the 2H to 1T' phase (for the three primary lattice distortions, see ‘‘Crystal Structures’’ in SUPPLEMENTARY INFORMATION). We calculate the potential energy as a function of displacement amplitude of these vibrations under different photoexcitation energies to investigate the phase instability. The results are summarized in Fig. 2(b)-(d), with the energy of the excited 1T' phase set as zero for comparing the relative stability between the 2H and 1T' phases. In the ground state, the energy of the 2H phase is 80 meV lower than that of the 1T' phase. However, as the system is optically excited, the 2H phase becomes energetically less favorable than the 1T' phase due to population inversion²², which is consistent with previous results²³.

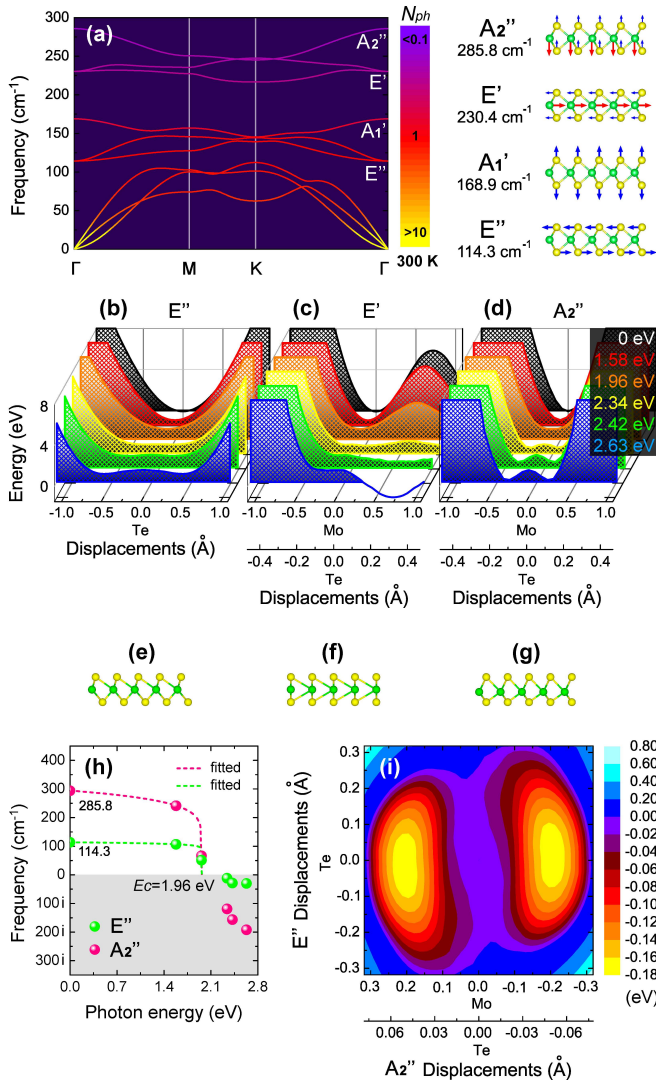


FIG. 2. (a) Phonon dispersion and vibrational modes for optical phonons at the Γ point. The phonon occupation number is determined from the Bose-Einstein distribution function at 300 K. Potential energy surface at different excitation energies along the eigenvectors of (b) E'' , (c) E' , and (d) A_2'' modes, and their corresponding structures (e)-(g) with a minimum energy at 2.63 eV. (h) Phonon frequency of the E'' and A_2'' modes as a function of laser excitation energy. (i) Energy surface in the plane spanned by the two soft modes. Each contour line represents an energy increase of 0.02 eV.

Under optical excitation, these three atomic displacements lead to structural phase transitions along the pathway from the 2H to 1T' phase. For the E'' mode (corresponding to the opposite in-plane motion of top and bottom Te layers), the Te atoms vibrate harmonically around their equilibrium positions before photoexcitation. With increasing excitation energy E , the potential energy surface gradually flattens, and a double-well potential forms at $E > 1.96$ eV. Thus a distorted octahedral structure can be formed as atoms move to new equilibrium positions [Fig. 2(e)]. A similar situation occurs for the A_2'' mode (an out-of-plane displacement of Mo atoms and an opposite-direction displacement of Te atoms).

For $E > 1.96$ eV, the Mo atoms can bounce up or down to the two minimum energy sites of the new double-well potential, while the Te atoms move in opposite directions, leading to an out-of-plane distorted variant of 2H MoTe₂ [Fig. 2(g)]. The evolution of the E' mode under irradiation is slightly different. This mode is composed of in-plane displacements with the one Mo layer and the two Te layers moving opposite to each other. Increasing E lowers the energy barrier for positive displacements along the eigenvector of the E' mode, and the barrier becomes a deep well at 2.63 eV, leading to atomic displacement in Fig. 2(f). After cessation of the excitation, such atomic displacement results in distorted in-plane atomic positions, yielding a twisted octahedral coordination around Mo atoms. All three displacements of the corresponding mode eigenvectors are along the phase transition pathway from 2H to 1T' MoTe₂.

The transition from a single-well potential to a double-well potential shown in Fig. 2(b)-(d) indicates a displacive phase transition, which involves a phonon frequency that falls to zero at a critical excitation energy E_C . These frozen-in modes are called soft modes, and the crystal becomes unstable against the displacements of the corresponding mode eigenvectors, leading to spontaneous symmetry breaking^{35,36}. We examine the soft-mode behaviour under optical excitation in the frame of Landau theory. For a soft mode displacive phase transition, the order parameter can be the amplitude of the distortion of the soft mode eigenvector³⁵. The lattice potential energy, equivalent to the free energy in the Landau theory^{37,38}, can be expressed by a fourth order even polynomial expansion of the order parameter u

$$V(u) = a + \frac{b}{2}u^2 + \frac{c}{4}u^4, \quad (2)$$

where the harmonic prefactor b is equivalent to the square of the soft mode phonon frequency ω ^{35,39}. Before the phase transition, there is a single-well potential, corresponding to $b > 0$ (c is a small positive value with a much weaker E dependence). When b becomes negative, $V(u)$ must be a double-well function with minima at $u = \pm\sqrt{-b/c}$ and a maximum value at $u = 0$. Thus the phonon softening can be described quantitatively by calculating the phonon frequencies of the E'' and A_2'' modes as a function of photoexcitation energy. As shown in Fig. 2(h), at 1.58 eV both modes soften slightly, and drop significantly at 1.96 eV. The phonon frequency becomes imaginary for $E > 1.96$ eV, confirming again that a soft mode phase transition occurs at $E > 1.96$ eV. We also calculate the energy surface in the subspace spanned by the soft modes⁴⁰ to see spontaneous lattice distortions. Fig. 2(i) shows the energy surface mapped on the plane spanned by the two soft modes E'' and A_2'' at the photoexcitation energy of 2.34 eV. All the displacements with energies lower than zero can lead to spontaneous symmetry breaking along the pathway from the 2H to 1T' phase, indicating a phase transition at this photoexcitation energy.

In the Landau theory, the phase transition occurs at $b = 0$. For temperature-driven ferroelectric/magnetic phase transitions, $b \propto (T - T_0)$, giving the well-known Curie-Weiss law³⁷. In the detailed analysis of the potential well of the E'' mode,

TABLE I. Excited carrier concentration n and the maximum amount of excitation N by a laser pulse with a fluence of 100 mJ/cm^2 , as well as their corresponding excitation percentage in the total number of valence electrons N_{tot} , at different laser excitation energies.

Energy (eV)	1.58	1.96	2.34	2.42	2.63
$n (\times 10^{14} \text{ cm}^{-2})$	0.9	3.4	10.1	11.8	13.2
$n/N_{\text{tot}} (\%)$	0.8	2.9	8.5	9.9	11.1
$N (\times 10^{14} \text{ cm}^{-2})$	7.2	12.2	16.0	17.2	17.6
$N/N_{\text{tot}} (\%)$	6.0	10.2	13.5	14.5	14.8

we find $b \propto (E_C - E)^\gamma$, where $E_C = 1.96 \text{ eV}$ and $\gamma = 0.077$. Since $b = \omega^2$, we fit the mode frequencies as a function of E by $\omega \propto (E_C - E)^{\gamma/2}$, as shown in Fig. 2(h). The obtained $E_C = 1.96 \text{ eV}$ is in good agreement with the change of electron distribution [Fig. 1(b) and (c)], from which one can see that the electron localization function essentially shows similar features for $E \geq 1.96 \text{ eV}$. Our prediction of photo-induced lattice mode softenings, marked by clear changes in both Raman and infrared spectra, can be easily verified experimentally by ultrafast coherent phonon spectroscopy²⁵ or second harmonic generation⁴¹.

For a thermally induced phase transition, $b = \tilde{b}(T - T_0)$, where \tilde{b} is a positive constant³⁵, the potential well changes gradually with temperature towards the phase transition. In contrast, in a photo-induced phase transition, the potential well change is determined by the number of excited carriers, which is related to the excitation energy E and the density of states (DOS) (discussed later in *Excited carrier concentrations*). For instance, when E is only slightly larger than the band gap, few electrons are excited to the conduction bands, leading to a negligible change of the potential well. Thus in the photo-induced phase transition, b has a much weaker E dependence than the T dependence in a thermally induced phase transition, leading to a much smaller γ .

Excited carrier concentrations. The population of the occupied conduction bands at different excitation energies is determined by energy conservation, the larger the excitation energies, the more electrons satisfy the energy conservation and hence are excited. Thus each excitation energy corresponds to a specific excited carrier concentration. Table I shows the excited carrier concentrations under different excitation energies. The excited carrier density at 1.96 eV is $3.4 \times 10^{14} \text{ cm}^{-2}$, corresponding to an excited carrier density of 2.9%. We also estimate the maximum amount of electron-hole pairs generated by a femtosecond laser with a fluence of 100 mJ/cm^2 [for the calculations of the maximum amount of electron-hole pairs, see “After Laser Excitation (within 20 fs)” in SUPPLEMENTARY INFORMATION]. As shown in Table I, at 1.96 eV up to 10.2% excitation is possible for a laser pulse with a fluence of 100 mJ/cm^2 . Thus the excited carrier concentrations in our calculations are reasonable estimates. As a PIPT can take place for excitations over 2.9%, a laser pulse with a minimum fluence of 28 mJ/cm^2 is needed to induce a phase transition at 1.96 eV . This is consistent with the experimental fact that with insufficient laser fluence, the phase transformation cannot take place completely even for long irradiation times^{9,19}.

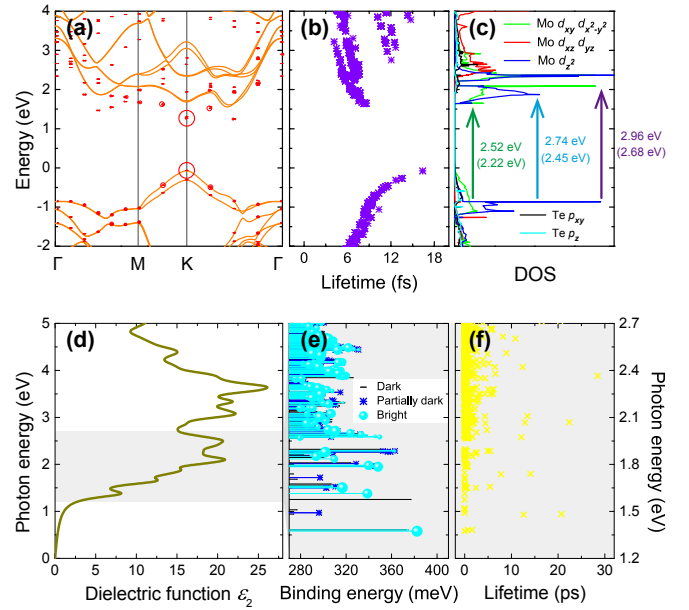


FIG. 3. (a) Electronic structures, (b) quasiparticle relaxation time, and (c) DOS of monolayer MoTe_2 . The red circles in (a) denote the first exciton. The radius of circles represents the electron-hole coupling coefficient of excitonic wave functions. The larger the radius, the more an electron-hole pair contributes to the exciton eigenstate. The arrows in (c) indicate optical transitions with different electronic excitation energies. The parentheses in (c) show the exciton excitation energies. (d) Imaginary part of dielectric function ϵ_2 , (e) dark, partially dark, and bright excitons with different binding energies, and (f) exciton lifetime for monolayer MoTe_2 . The radius of circles in (e) represents the oscillator strength for bright excitons.

The excited carrier population is related to the DOS⁴². Our calculated electronic structure [Fig. 3(a)] agrees well with previous results^{43,44} (for details on the band gap and spin splitting, see “Electronic Structure and Optical Properties” in SUPPLEMENTARY INFORMATION). As marked by arrows in Fig. 3(c), optical transitions between the DOS peaks correspond to the excitation energies of 2.52 eV , 2.74 eV , and 2.96 eV . In 2D materials, reduced electronic screening typically leads to strong excitonic effect⁴⁵. By including electron-hole interactions, the calculated imaginary part of dielectric function ϵ_2 shows a non-zero value above a photon energy of 1.0 eV [Fig. 3(d)], which agrees well with optical absorption measurements⁴⁶. Because of the electron-hole attraction, the optical transition energies between the DOS peaks are reduced to 2.22 eV , 2.45 eV , and 2.68 eV [shown in parentheses in Fig. 3(c)]. With laser energies larger than 2.22 eV , the concentrations of excited carriers become higher, corresponding to strong optical excitation.

Timescale of the phase transition. The timescale after laser excitation is divided into three regimes.

In the first stage, the temperature of the electronic systems increases rapidly as electrons thermalize within 20 fs , while the lattice remains cold. In photoexcited MoTe_2 , carrier-carrier scattering is responsible for redistributing carrier energy, resulting in a thermalized distribution function of

carriers²⁴. The carrier relaxation time can be calculated from the quasiparticle self-energy^{45,47}. As shown in Fig. 3(b), the excited electrons thermalize in 20 fs. The lifetime of these excited electrons, equivalent to the electron-hole recombination time, is calculated from the electron-hole amplitude and the quasiparticle self-energy^{45,48}. As shown in Fig. 3(f), the recombination occurs on the order of picoseconds. Thus in the first stage (within 20 fs), all the excited electrons are in thermal equilibrium before interacting with phonons.

In the second stage, the symmetry breaking displacements in 2H MoTe₂ take place within 292 fs. As the laser pulse creates electronic excitations, the new potential energy surfaces in Fig. 2(b)-(d) are formed immediately. The photo-induced lattice distortions, as a result of phonon softening, occur within the timescale of lattice vibrations. This can be estimated by the lattice vibration period from 117 fs (A₂' mode) to 292 fs (E'' mode). Such an estimate agrees well with previous molecular dynamics simulations²² and pump-probe spectroscopy²⁵. Because the timescale for carrier-phonon interaction is 1-100 ps²⁴, the structural distortion can take place before the electrons transfer their energy to the lattice.

In the third stage, the hot carriers are cooled by transferring energy to the lattice, converting electronic photoexcitation energy to heat in hundreds of picoseconds through interaction with various phonons. Some argue that, after the excited electrons are instantly relaxed to lattice heat through electron-phonon coupling, atomic reorganization toward the 1T' phase may occur as a result of local heat¹⁷ or thermal strain^{20,21}. We demonstrate that these thermal effects alone cannot trigger the phase transition: only at temperatures higher than 930 K does the 1T' MoTe₂ phase become thermodynamically more stable than the 2H phase [for the calculations of thermodynamic stability, see “Thermal Effects (about hundreds of ps)” in SUPPLEMENTARY INFORMATION]. This is consistent with the experimental evidence that the pure 1T' phase appears at 930 K under Te deficiency³⁰. However, the temperature necessary to

induce this phase transition, 930 K, is much higher than the laser-induced temperature of 670 K⁹. Even after taking thermal strain into consideration, the phase transition temperature of 810 K is still higher than the laser-induced temperature [for the role of thermal strain, see “Thermal Effects (about hundreds of ps)” in SUPPLEMENTARY INFORMATION]. Therefore the laser-induced thermal effect on the phase transition is probably overestimated in earlier studies^{9,17}.

In summary, we demonstrate that a sub-picosecond phase transition in monolayer MoTe₂ from the 2H phase to a distorted 1T' phase can be triggered by purely electronic excitation, even when the lattice is still cold. Such electronic excitation changes the electron density, resulting in a soft mode displacive phase transition. The phase transition from the room-temperature 2H phase to the high-temperature 1T' phase can be induced by a critical excitation energy of 1.96 eV, at which 2.9% of the carriers are excited. We also show that this phase transition mechanism can be understood in the frame of the Landau theory, and is quite different from the temperature-driven phase transition. Our findings shed new light on the microscopic origin of PIPT in 2D transition-metal ditellurides, and are expected to trigger both fundamental and applied studies on ultrafast phase transition in these new class materials such as topological switching and neuromorphic computing.

The authors gratefully acknowledge helpful discussions with Ms. Fangyuan Gu at Imperial College London and Prof. Xian-Bin Li at Jilin University. This work is supported by the National Natural Science Foundation of China under Grants No. 11374063, 11674369, 11404348 and 61774042, the National Key Research and Development Program of China (No. 2016YFA0300600 and 2018YFA0305700), the “Strategic Priority Research Program (B)” of the Chinese Academy of Sciences (Grant No. XDB07020100), and MEXT KAKENHI Grant Number JP17K05031, and Shanghai Municipal Natural Science Foundation (19ZR1402900, 17ZR1446500).

* zhangh@fudan.edu.cn

† fu.tokusho@shizuoka.ac.jp

‡ hmweng@iphy.ac.cn

¹ K. Nasu, ed., *Photo-induced phase transitions* (World Scientific, 2004).

² H. K. Bisoyi and Q. Li, *Chem. Rev.* **116**, 15089 (2016).

³ J. M. Wu and L. B. Liou, *J. Mater. Chem.* **21**, 5499 (2011).

⁴ S. Koshihara, Y. Tokura, T. Mitani, G. Saito, and T. Koda, *Phys. Rev. B* **42**, 6853 (1990).

⁵ E. Hanamura, in *Relaxations of Excited States and Photo-Induced Structural Phase Transitions* (Springer Berlin Heidelberg, Berlin, Heidelberg, 1997) pp. 34–44.

⁶ Y. Wang, J. Xiao, H. Zhu, Y. Li, Y. Alsaïd, K. Y. Fong, Y. Zhou, S. Wang, W. Shi, Y. Wang, A. Zettl, E. J. Reed, and X. Zhang, *Nature* **550**, 487 (2017).

⁷ Z. Fei, W. Zhao, T. A. Palomaki, B. Sun, M. K. Miller, Z. Zhao, J. Yan, X. Xu, and D. H. Cobden, *Nature* **560**, 336 (2018).

⁸ F. Zhang, H. Zhang, S. Krylyuk, C. A. Milligan, Y. Zhu, D. Y. Zemlyanov, L. A. Bendersky, B. P. Burton, A. V. Davydov, and J. Appenzeller, *Nature Materials* **18**, 55 (2019).

⁹ S. Cho, S. Kim, J. H. Kim, J. Zhao, J. Seok, D. H. Keum, J. Baik, D.-H. Choe, K. J. Chang, K. Suenaga, S. W. Kim, Y. H. Lee, and H. Yang, *Science* **349**, 625 (2015).

¹⁰ E. J. Sie, C. M. Nyby, C. D. Pemmaraju, S. J. Park, X. Shen, J. Yang, M. C. Hoffmann, B. K. Ofori-Okai, R. Li, A. H. Reid, S. Weathersby, E. Mannebach, N. Finney, D. Rhodes, D. Chenet, A. Antony, L. Balicas, J. Hone, T. P. Devereaux, T. F. Heinz, X. Wang, and A. M. Lindenberg, *Nature* **565**, 61 (2019).

¹¹ H. Yang, S. W. Kim, M. Chhowalla, and Y. H. Lee, *Nature Physics* **13**, 931 (2017).

¹² X. Qian, J. Liu, L. Fu, and J. Li, *Science* **346**, 1344 (2014).

¹³ D.-H. Choe, H.-J. Sung, and K. J. Chang, *Phys. Rev. B* **93**, 125109 (2016).

¹⁴ E. Sajadi, T. Palomaki, Z. Fei, W. Zhao, P. Bement, C. Olsen, S. Luescher, X. Xu, J. A. Folk, and D. H. Cobden, *Science* **362**, 922 (2018).

¹⁵ V. Fatemi, S. Wu, Y. Cao, L. Brethau, Q. D. Gibson, K. Watanabe, T. Taniguchi, R. J. Cava, and P. Jarillo-Herrero, *Science* **362**, 926 (2018).

¹⁶ S. Kretschmer, H.-P. Komsa, P. Boggild, and A. V. Krashenin-

- nikov, J. Phys. Chem. Lett. **8**, 3061 (2017).
- ¹⁷ Z. Wang, X. Li, G. Zhang, Y. Luo, and J. Jiang, ACS Appl. Mater. Interfaces **9**, 23309 (2017).
 - ¹⁸ A. Yoshimura, M. Lamparski, N. Kharche, and V. Meunier, Nanoscale **10**, 2388 (2018).
 - ¹⁹ Y. Tan, F. Luo, M. Zhu, X. Xu, Y. Ye, B. Li, G. Wang, W. Luo, X. Zheng, N. Wu, Y. Yu, S. Qin, and X.-A. Zhang, Nanoscale **10**, 19964 (2018).
 - ²⁰ K.-A. N. Duerloo, Y. Li, and E. J. Reed, Nature Communications **5**, 4214 (2014).
 - ²¹ S. Song, D. H. Keum, S. Cho, D. Perello, Y. Kim, and Y. H. Lee, Nano Lett. **16**, 188 (2016).
 - ²² A. V. Kolobov, P. Fons, and J. Tominaga, Phys. Rev. B **94**, 094114 (2016).
 - ²³ A. Krishnamoorthy, L. Bassman, R. K. Kalia, A. Nakano, F. Shimojo, and P. Vashishta, Nanoscale **10**, 2742 (2018).
 - ²⁴ J. Shah, *Ultrafast spectroscopy of semiconductors and semiconductor nanostructures* (Springer Science & Business Media, 2013).
 - ²⁵ M. Y. Zhang, Z. X. Wang, Y. N. Li, L. Y. Shi, D. Wu, T. Lin, S. J. Zhang, Y. Q. Liu, Q. M. Liu, J. Wang, T. Dong, and N. L. Wang, Phys. Rev. X **9**, 021036 (2019).
 - ²⁶ H.-J. Kim, S.-H. Kang, I. Hamada, and Y.-W. Son, Phys. Rev. B **95**, 180101 (2017).
 - ²⁷ G. Kresse and J. Furthmüller, Phys. Rev. B **54**, 11169 (1996).
 - ²⁸ X.-B. Li, X. Q. Liu, X. Liu, D. Han, Z. Zhang, X. D. Han, H.-B. Sun, and S. B. Zhang, Phys. Rev. Lett. **107**, 015501 (2011).
 - ²⁹ N.-K. Chen, D. Han, X.-B. Li, F. Liu, J. Bang, X.-P. Wang, Q.-D. Chen, H.-Y. Wang, S. Zhang, and H.-B. Sun, Phys. Chem. Chem. Phys. **19**, 24735 (2017).
 - ³⁰ D. H. Keum, S. Cho, J. H. Kim, D.-H. Choe, H.-J. Sung, M. Kan, H. Kang, J.-Y. Hwang, S. W. Kim, H. Yang, K. J. Chang, and Y. H. Lee, Nature Physics **11**, 482 (2015).
 - ³¹ H. A. Jahn and E. Teller, Proceedings of the Royal Society of London. Series A, Mathematical and Physical Sciences **161**, 220 (1937).
 - ³² M. Yamamoto, S. T. Wang, M. Ni, Y.-F. Lin, S.-L. Li, S. Aikawa, W.-B. Jian, K. Ueno, K. Wakabayashi, and K. Tsukagoshi, ACS Nano **8**, 3895 (2014).
 - ³³ M. Kan, H. G. Nam, Y. H. Lee, and Q. Sun, Phys. Chem. Chem. Phys. **17**, 14866 (2015).
 - ³⁴ H. Guo, T. Yang, M. Yamamoto, L. Zhou, R. Ishikawa, K. Ueno, K. Tsukagoshi, Z. Zhang, M. S. Dresselhaus, and R. Saito, Phys. Rev. B **91**, 205415 (2015).
 - ³⁵ M. T. Dove, *Introduction to Lattice Dynamics* (Cambridge University Press, 1993).
 - ³⁶ M. T. Dove, American Mineralogist **82**, 213 (1997).
 - ³⁷ C. Kittel, *Introduction to solid state physics* (Wiley New York, 1976).
 - ³⁸ B. Zeks and R. Blinc, *Soft Modes in Ferroelectrics and Antiferroelectrics* (North-Holland, 1974).
 - ³⁹ B. Monserrat, Journal of Physics: Condensed Matter **30**, 083001 (2018).
 - ⁴⁰ J. C. A. Prentice, B. Monserrat, and R. J. Needs, Phys. Rev. B **95**, 014108 (2017).
 - ⁴¹ Y. Song, R. Tian, J. Yang, R. Yin, J. Zhao, and X. Gan, Advanced Optical Materials **6**, 1701334 (2018).
 - ⁴² M. Bernardi, D. Vigil-Fowler, J. Lischner, J. B. Neaton, and S. G. Louie, Phys. Rev. Lett. **112**, 257402 (2014).
 - ⁴³ A. Ramasubramaniam, Phys. Rev. B **86**, 115409 (2012).
 - ⁴⁴ C. Ruppert, O. B. Aslan, and T. F. Heinz, Nano Lett. **14**, 6231 (2014).
 - ⁴⁵ B. Peng, H. Zhang, H. Shao, K. Xu, G. Ni, L. Wu, J. Li, H. Lu, Q. Jin, and H. Zhu, ACS Photonics **5**, 4081 (2018).
 - ⁴⁶ I. G. Lezama, A. Arora, A. Ubaldini, C. Barreateau, E. Giannini, M. Potemski, and A. F. Morpurgo, Nano Lett. **15**, 2336 (2015).
 - ⁴⁷ T. Kotani and M. van Schilfgarde, Phys. Rev. B **81**, 125201 (2010).
 - ⁴⁸ K. F. Mak, F. H. da Jornada, K. He, J. Deslippe, N. Petrone, J. Hone, J. Shan, S. G. Louie, and T. F. Heinz, Phys. Rev. Lett. **112**, 207401 (2014).